

Time-resolved photoluminescence of lithographically defined quantum dots fabricated by electron beam lithography and wet chemical etching

V. B. Verma, Martin J. Stevens, K. L. Silverman, N. L. Dias, A. Garg, J. J. Coleman, and R. P. Mirin

Citation: *Journal of Applied Physics* **109**, 123112 (2011); doi: 10.1063/1.3599889

View online: <http://dx.doi.org/10.1063/1.3599889>

View Table of Contents: <http://scitation.aip.org/content/aip/journal/jap/109/12?ver=pdfcov>

Published by the [AIP Publishing](#)

Articles you may be interested in

[In situ electron-beam lithography of deterministic single-quantum-dot mesa-structures using low-temperature cathodoluminescence spectroscopy](#)

Appl. Phys. Lett. **102**, 251113 (2013); 10.1063/1.4812343

[Photoluminescence from GaAs nanodisks fabricated by using combination of neutral beam etching and atomic hydrogen-assisted molecular beam epitaxy regrowth](#)

Appl. Phys. Lett. **101**, 113108 (2012); 10.1063/1.4752233

[The effect of growth temperature of GaAs nucleation layer on InAs/GaAs quantum dots monolithically grown on Ge substrates](#)

Appl. Phys. Lett. **100**, 052113 (2012); 10.1063/1.3682314

[High density patterned quantum dot arrays fabricated by electron beam lithography and wet chemical etching](#)

Appl. Phys. Lett. **93**, 111117 (2008); 10.1063/1.2981207

[Fabrication of one-dimensional GaAs channel-coupled InAs quantum dot memory device by selective-area metal-organic vapor phase epitaxy](#)

Appl. Phys. Lett. **87**, 193103 (2005); 10.1063/1.2120905



Re-register for Table of Content Alerts

Create a profile.



Sign up today!



Time-resolved photoluminescence of lithographically defined quantum dots fabricated by electron beam lithography and wet chemical etching

V. B. Verma,^{1,a)} Martin J. Stevens,¹ K. L. Silverman,¹ N. L. Dias,² A. Garg,² J. J. Coleman,² and R. P. Mirin¹

¹*Optoelectronics Division, National Institute of Standards and Technology, Boulder, Colorado 80305, USA*

²*Department of Electrical and Computer Engineering, University of Illinois, Urbana, Illinois 61801, USA*

(Received 28 February 2011; accepted 10 May 2011; published online 29 June 2011)

We measure the time-resolved photoluminescence characteristics of a novel type of lithographically patterned quantum dot fabricated by electron beam lithography, wet chemical etching, and overgrowth of the barrier layers by metalorganic chemical vapor deposition. We find that the quantum dot (QD) photoluminescence exhibits a bi-exponential decay that we explain in terms of the fast capture of carriers by defect states followed by a slower radiative relaxation process. We also perform a systematic investigation of the rise time and decay time as a function of the QD density, size, and temperature. These measurements indicate that the carrier capture process in this type of QD is limited by carrier drift within the GaAs barrier material.

© 2011 American Institute of Physics. [doi:10.1063/1.3599889]

I. INTRODUCTION

Epitaxial quantum dots (QDs) formed by self-assembly have found many applications in optoelectronics including semiconductor lasers¹ and single-photon emitters.²⁻⁴ These QDs are formed by the intrinsic strain that exists between the material of the QD and the substrate material, resulting in a transition from two-dimensional planar epitaxial growth to the nucleation of three-dimensional islands. The decay time of the luminescence from these QDs is important because it sets an upper limit on the modulation speed of any device incorporating the QDs as an active material.

The QDs formed by the self-assembly technique nucleate in random positions and typically have a large inhomogeneous size distribution. For many applications, such as the deterministic coupling of a QD to an optical microcavity, it is desirable to have better control over the positions and sizes of individual QDs. In recent work, we have explored a QD fabrication technique that involves the use of electron beam lithography, wet chemical etching, and overgrowth of the barrier layers.⁵⁻⁷ This technique allows the properties of individual QDs, such as position and size, to be controlled. The use of metalorganic chemical vapor deposition (MOCVD) for the regrowth of the barrier layers has facilitated the incorporation of these QDs into semiconductor laser devices.⁶ More recently, we demonstrated that a single patterned QD (PQD) behaves as a single quantum emitter and is capable of producing single photons.⁷

We report on our investigation of the rise and decay times of the photoluminescence from PQDs. We observe a bi-exponential decay, which we explain in terms of the fast capture of photogenerated carriers by defect states followed by the slower radiative relaxation of the remaining carriers and repopulation of the QD states from the barrier. We also systematically investigate the effect of the QD density and

size, both of which can be lithographically defined, along with the temperature, on the rise and decay times of the photoluminescence.

II. EXPERIMENT

The fabrication process begins with a base structure grown by molecular beam epitaxy (MBE) on an undoped (100) GaAs substrate and consists of a 20-period GaAs/AlAs distributed Bragg reflector stack for increasing the extraction efficiency of light emitted from the QDs, a 130 nm GaAs lower core, an 8 nm In_{0.2}Ga_{0.8}As quantum well, and a 10 nm GaAs cap.

Electron beam lithography was performed with a scanning electron microscope with an acceleration voltage of 30 kV and beam current of 20 pA. Polymethyl methacrylate (PMMA) was used as the electron beam resist. Regular arrays of dots were patterned in square lattices with various pitches ranging from 500 nm to 5 μ m. The dot diameters were also varied by modifying the electron beam dose. After development, 20 nm of titanium metal was evaporated on the sample, followed by lift-off in acetone. The metal dot patterns were then transferred into the underlying quantum well layer in a solution of 1:4:495 H₃PO₄:H₂O₂:H₂O for 40 s to provide an etch depth of 25 nm. After etching, the titanium was stripped in buffered hydrofluoric acid for 1 min. Figure 1 shows an array of 45 nm diameter QDs on a 1 μ m pitch after the etch mask had been stripped. Following the etching step, the barrier layers were regrown in a low-pressure MOCVD reactor and consist of a 130 nm GaAs upper core, an 80 nm AlAs confinement layer, and a 10 nm GaAs cap.

Optical measurements were performed at temperatures ranging from 4 to 100 K in a liquid helium cryostat. A mode-locked Ti:sapphire laser (795 nm wavelength, 82 MHz repetition rate) was used as the excitation source. The pump beam was focused down to a spot size of approximately 4 μ m with a 0.6 numerical aperture objective. All pump

^{a)}Electronic mail: verma@nist.gov.

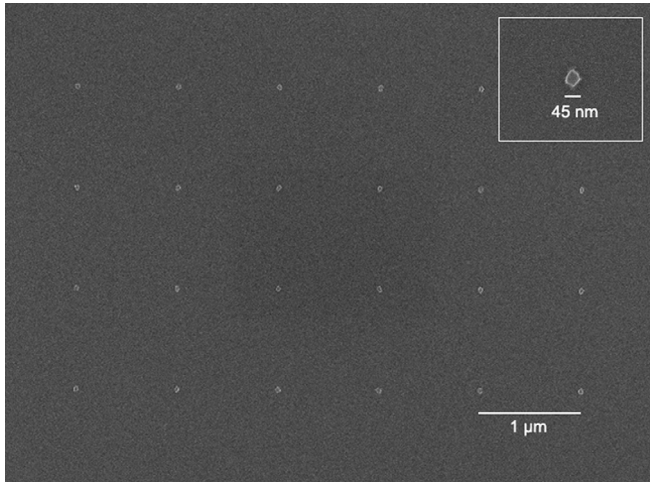


FIG. 1. An array of 45 nm diameter etched QDs on a pitch of 1 μm . The inset shows a magnified image of a single QD.

powers reported here are time-average powers. For reference, in the following measurements, a time-average pump power of 100 nW corresponds to a photogenerated carrier density of approximately 5×10^{14} electron-hole pairs per pump pulse, and a fluence of 8 kW/cm^2 . Light emitted from the QDs was collected by the same objective and focused onto the input slit of a 0.75 m focal length monochromator. An internal mirror in the monochromator was used to switch between a liquid nitrogen-cooled CCD camera for recording emission spectra and a single-photon avalanche diode (SPAD) for the measurement of the time-resolved characteristics of the photoluminescence using the time-correlated single-photon counting technique. Timing electronics were used to generate the photoluminescence decay curves, with the start signal provided by a fast photodiode triggered off of the Ti:sapphire laser pulse and the stop signal provided by the SPAD. The rise and decay times of the QD photoluminescence were computed after deconvolution with the measured instrument response.

III. RESULTS AND DISCUSSION

A. Time-resolved photoluminescence from a single PQD

Figure 2 shows the emission spectrum obtained at 4 K from a lithographically defined QD array with a pitch of $2.5 \mu\text{m}$ and a QD diameter of 35 nm. Since the pitch is larger than the radius of the pump spot, we are primarily exciting a single QD in this array. The linewidth of this particular QD is 0.16 nm or $260 \mu\text{eV}$. Measurement of the second-order correlation function at zero time delay on this particular QD resulted in a value of $g^{(2)}(0) = 0.395 \pm 0.030$, demonstrating that it is acting as a source of single photons.⁷ Figure 3 shows the photoluminescence decay for this particular emission line at time-average pump powers between 100 nW and $1 \mu\text{W}$. The spectrometer was set to pass a spectral bandwidth of $\sim 0.2 \text{ nm}$ for these measurements, approximately equal to the linewidth of the QD emission.

Figure 4 shows the rise and decay time constants measured after deconvolution of the time-resolved photolumines-

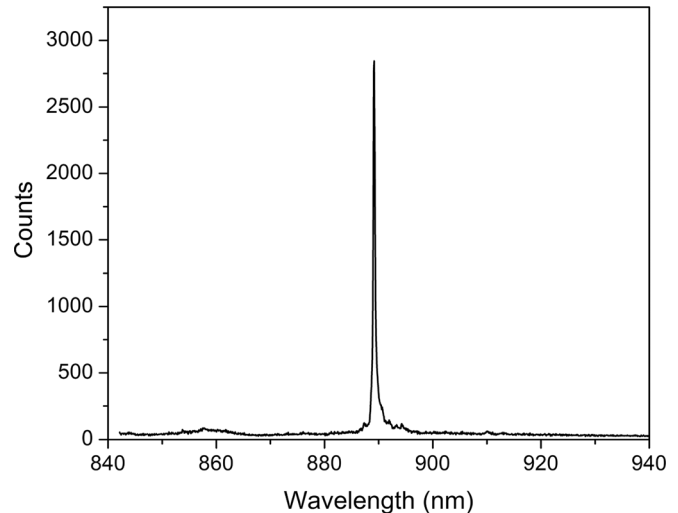


FIG. 2. Emission spectrum of a single 35 nm diameter QD.

cence (TRPL) traces in Fig. 3 from the instrument response. In this report, most measurements of the rise and decay time have an uncertainty on the order of $\pm 10 \text{ ps}$. We observe rise times ranging between 150 and 200 ps, which is significantly longer than the rise times observed with self-assembled QDs (SAQDs), which are typically on the order of 10–100 ps.^{8,9} We also note a trend of increasing rise time with increasing pump power. In contrast, self-assembled QDs typically exhibit a decrease in rise time with increasing pump power, which is generally attributed to the Auger processes.^{8,9}

The short decay time constant ranges between 300 and 400 ps, and also shows a trend of increasing as the pump power is increased. This fast decay is not observed with self-assembled QDs, which generally have a mono-exponential decay with a time constant of approximately 1 ns. The time constant of the long tail of the PL as shown in Fig. 3 ranges from 2.0–2.5 ns. As we will show, the fast decay can be

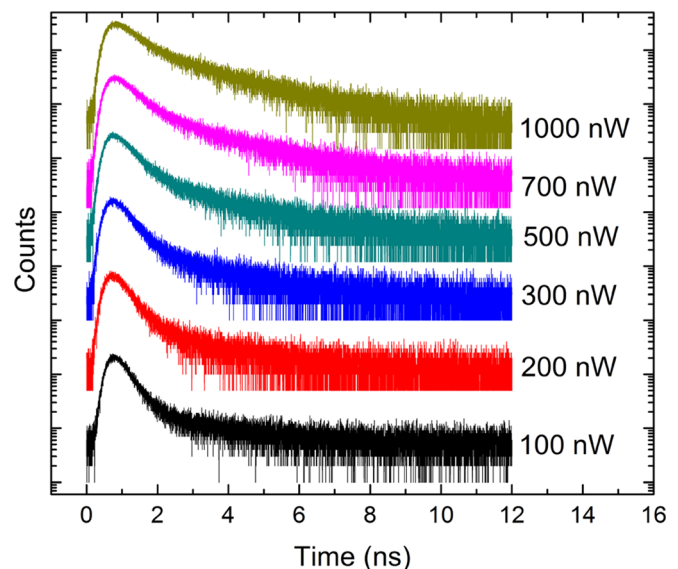


FIG. 3. (Color online) Time-resolved photoluminescence at pump powers between 100 nW and 1000 nW of the exciton line at 888.6 nm in Fig. 2.

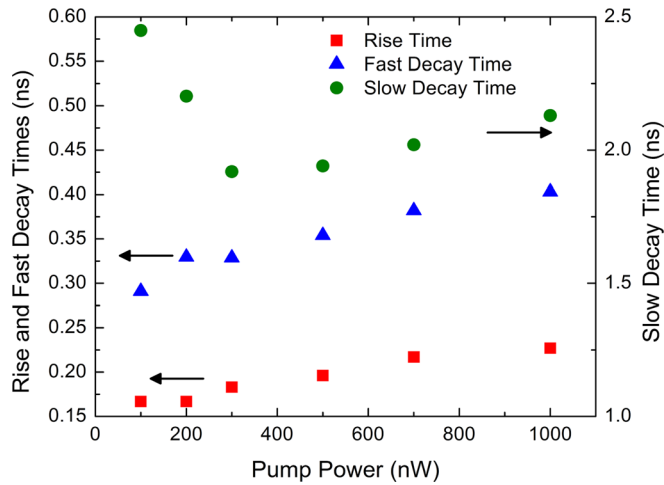


FIG. 4. (Color online) Rise time, fast decay time, and slow decay time measured on the single QD emission in Fig. 2.

attributed to the capture of the carriers by defect states, while the long tail is likely due to the radiative recombination of the remaining carriers. The sharp increase in the slow decay time below 300 nW in Fig. 4 may be due to the low power and low QD density, which results in less than one electron-hole pair, on average, being captured by the QD per pulse. In this regime the long tail of the PL consists of the time it takes for an electron-hole pair to be captured, which may be comparable to the radiative lifetime itself, plus the radiative lifetime. At higher pump powers the capture time is significantly reduced and the time constant of the long tail becomes dominated by the radiative lifetime.

In the following, we perform a systematic investigation of the PL rise and decay times as a function of the QD density and size in order to better understand the observed trends in the data in Figs. 3 and 4.

B. Rise time of PQD ensembles

The rise time of the QD PL is determined by two processes: the relaxation of carriers from the GaAs barrier into the QD, and the subsequent relaxation between quantized states of the QD itself. Self-assembled QDs typically lie above a thin two-dimensional wetting layer. The photogenerated carriers may either be captured first by the wetting layer and then by the QDs, or directly from the barrier into the QDs. Detailed theoretical and experimental analyses of the capture process have shown that the wetting layer acts as an efficient decay pathway for relaxation from the barrier into the QDs, resulting in short capture times on the order of tens of picoseconds.^{9–11} The PQDs are unique in the fact that there is no two-dimensional wetting layer to aid in the capture of carriers, which in this case must relax directly into the QDs from the GaAs barrier. In addition, we note that QD densities explored in this work range between $4 \times 10^6 \text{ cm}^{-2}$ and $4 \times 10^8 \text{ cm}^{-2}$, which are significantly lower than SAQD densities which typically range between $1 \times 10^{10} \text{ cm}^{-2}$ and $1 \times 10^{11} \text{ cm}^{-2}$. Both the lack of a wetting layer and the lower QD densities may contribute to significant differences in the

carrier capture rates and hence, the PL rise times of the lithographically defined QDs compared to SAQDs.

The efficiency with which carriers are transferred from the barrier into the QDs can be gauged by comparing the decay time of the GaAs emission in a region with QDs and a region without QDs. If the capture process is efficient the decay time of the GaAs PL should be faster in an area patterned with QDs compared to a region without QDs. Figure 5 shows a comparison of the TRPL traces from a region on the sample that has been patterned with a high-density array of QDs 80 nm in diameter on a pitch of $0.5 \mu\text{m}$ and a region where the quantum well has been completely etched away, leaving only the GaAs barrier. The traces were fitted by single exponential decays yielding time constants of $1.302 \pm 0.016 \text{ ns}$ for the area patterned with QDs and $1.355 \pm 0.015 \text{ ns}$ for the unpatterned area. The small difference in the decay times between the patterned and unpatterned areas implies that the majority of carriers recombine in the GaAs barrier before being captured by the QDs. This is in contrast to SAQDs, which result in a drastic decrease in the GaAs decay time-constant compared to a region where the QDs have been etched away.⁸

The lithographic patterning process allows the QD density and size to be systematically varied, which allows us to better characterize and understand the carrier capture process. Figure 6 shows the emission spectra from four different ensembles of PQDs with pitches of 0.5, 1, 1.6, and $5 \mu\text{m}$, corresponding to densities of $4 \times 10^8 \text{ cm}^{-2}$, $1 \times 10^8 \text{ cm}^{-2}$, $3.9 \times 10^7 \text{ cm}^{-2}$, and $4 \times 10^6 \text{ cm}^{-2}$. Each ensemble consists of circular QDs approximately 80 nm in diameter. Small deviations in the ground-state emission wavelength between arrays are likely caused by small deviations in the diameter and shape of the QDs in each array. Since the diameter of the pump beam is approximately $4 \mu\text{m}$, at a pitch of $5 \mu\text{m}$ we are isolating the emission from a single PQD. Figure 7 shows the rise times measured at the peak of the QD luminescence as a function of pump power for each of the four QD

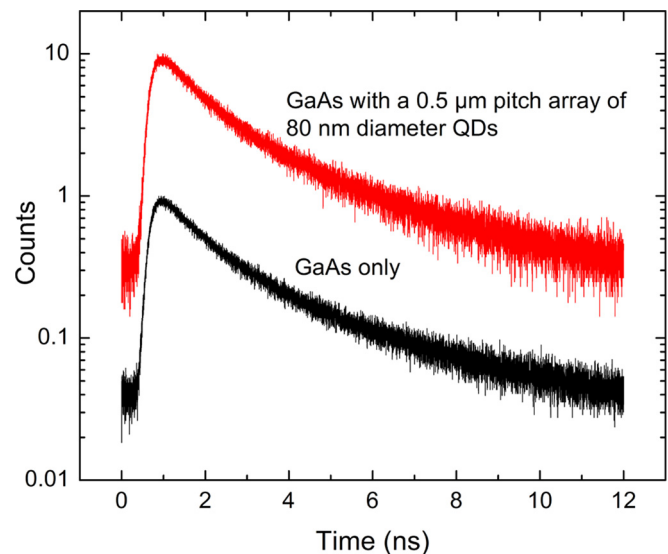


FIG. 5. (Color online) TRPL traces of emission from the GaAs barrier in a region that has been patterned with a high density array of QDs and a region with no QDs.

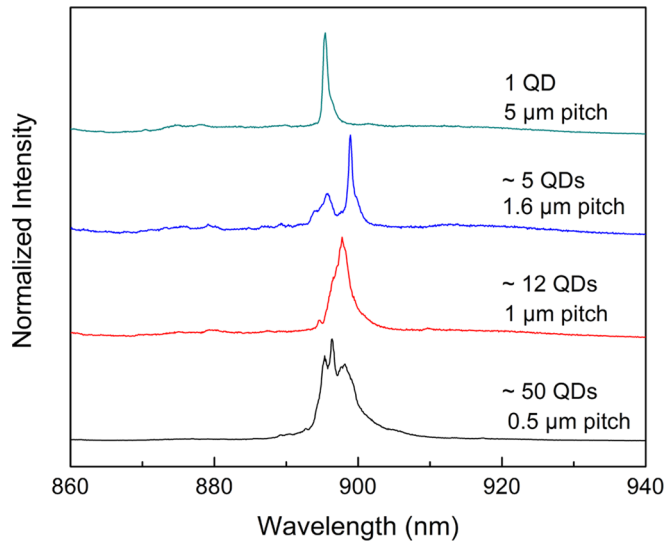


FIG. 6. (Color online) Sample emission spectra of QD ensembles with varied pitch and fixed QD diameter of 80 nm. Spectra were obtained at a pump power of 100 nW.

densities. The spectrometer was set to pass a spectral bandwidth of ~ 0.4 nm.

We observe two distinct trends in the rise times of these ensembles. First, for a fixed density, the rise time increases with increasing pump power. Second, for a fixed pump power, the rise time increases as the density is decreased. This trend is consistent with measurements performed on SAQD samples with different QD densities.¹²

To explain the increase in the rise time with pump power, we note that increasing the pump power leads to bandfilling of the excited states of the QD. Carriers in these excited states may later relax into the lower energy states, leading to an increase in the rise time. We also note that at high pump powers the rise times of the QD arrays with pitches of 0.5, 1, and 1.6 μm exhibit a saturation behavior that can be attributed to the more efficient capture rate of these high-density arrays. The rise time of the 5 μm pitch

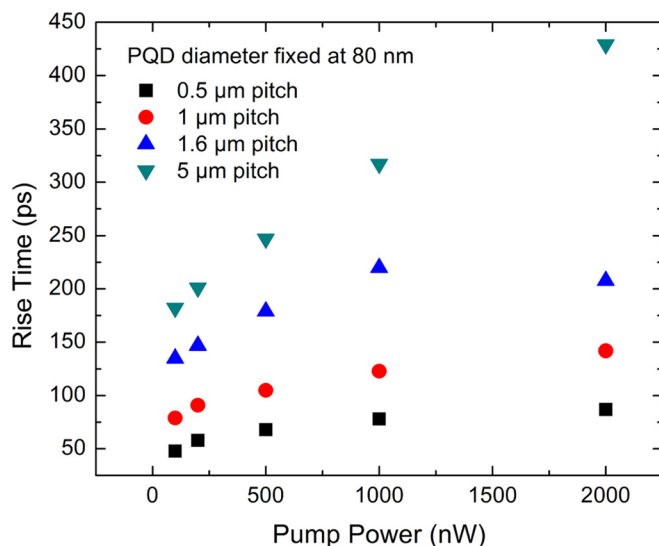


FIG. 7. (Color online) Rise time of QD ensembles with varied pitch and fixed QD diameter of 80 nm as a function of pump power.

array remains linear even at the highest pump power measured, which indicates a significantly lower capture rate in such a low-density array.

Without developing a full quantum mechanical model for the process of carrier capture, we should qualitatively expect the rate of carrier capture to be proportional to the fill factor of the QD array, which we define as,

$$\eta = A_{\text{QD}} \cdot \rho, \quad (1)$$

where A_{QD} is the area occupied by a single QD and ρ is the QD density. The carrier capture rate and capture time constant can then be expressed as,

$$r \propto \eta N_b v_{\text{th}}, \quad (2)$$

and

$$\tau \propto 1/(\eta N_b v_{\text{th}}), \quad (3)$$

respectively, where v_{th} is the thermal velocity of photogenerated carriers in the barrier given by $v_{\text{th}} = (3k_b T/m^*)^{1/2}$, where m^* is the effective mass of the carrier, k_b is Boltzmann's constant, T is the temperature, and N_b is the carrier density in the barrier. Note that due to the larger effective mass of the heavy hole compared to the electron, the hole diffusion will be the limiting factor in the rise time. Figure 8 shows the rise time as a function of the inverse fill factor. According to Eq. (3) we should expect the rise time to be linear with the inverse fill factor. From Fig. 8 we note that this is approximately true for the three smallest values of the inverse fill factor. The slight nonlinearity is likely caused by the saturation effect, which occurs for arrays with a high fill factor, as previously discussed. The array with the largest inverse fill factor (largest pitch of 5 μm) significantly deviates from a straight-line fit of the data from the higher-density arrays. To explain this saturation effect of the rise time with decreasing density, we note that Eqs. (2) and (3) do not take into account recombination within the GaAs that

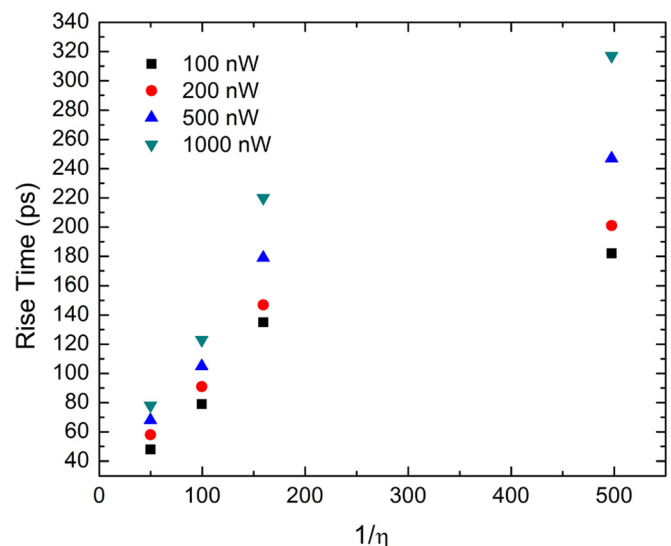


FIG. 8. (Color online) Rise time plotted as a function of inverse fill factor for four different pump powers.

competes with the QD carrier capture process. Carriers generated within the GaAs barrier will have a characteristic diffusion length before recombining in the GaAs. Although the lack of data for pitches between 1.6 and 5 μm makes it difficult to accurately determine this diffusion length, the data in Fig. 8 suggests that 1.6 μm can be taken as a reasonable lower bound. The QD arrays with pitches larger than this characteristic length will exhibit a significantly reduced capture efficiency, leading to a saturation of the rise time.

In addition to the dependence of the rise time on the density of the QD array, we also investigated the dependence of the rise time on the size of the QDs in the array, keeping the density fixed. Each array has a pitch of 0.5 μm , corresponding to a density of $4 \times 10^8 \text{ cm}^{-2}$. The diameters of the QDs in the three arrays were defined to be 80, 65, and 40 nm. Figure 9 shows the spectra obtained from these three arrays at a pump power of 100 nW. The blueshift of the ground-state emission wavelength with decreasing QD size is consistent with the strain and quantum confinement effects that we have observed in previous work.^{5,6} Figure 10 shows the rise times of the PL from these three arrays as a function of pump power. We again find that the rise times increase with increasing pump power, which is consistent with the data in Fig. 7. More importantly, the rise times are strongly dependent on the QD size, with the smaller diameter QDs having longer rise times.

There are two possible explanations for this trend. The first is that the smaller QDs simply present a smaller capture cross section and hence a smaller η [Eq. (1)], which reduces the capture efficiency. The second possibility is that the carrier capture rate from the barrier is unchanged, while the relaxation rate between discrete states within the QD itself is reduced as the QD size is reduced. A reduced intra-band relaxation rate has been theoretically predicted for QDs due to the requirement of matching the energy difference between quantized levels with the energy of an acoustic phonon, which is an effect that has become known as the phonon

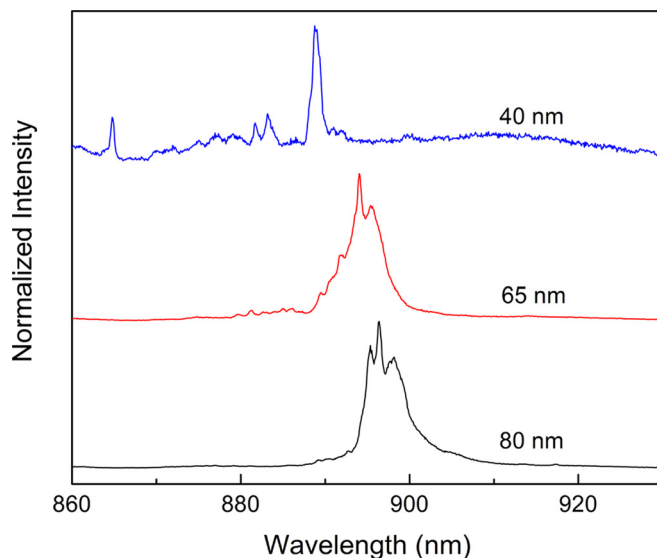


FIG. 9. (Color online) Sample emission spectra obtained at a pump power of 100 nW from three QD arrays with the same density and different QD diameters of 80, 65, and 40 nm.

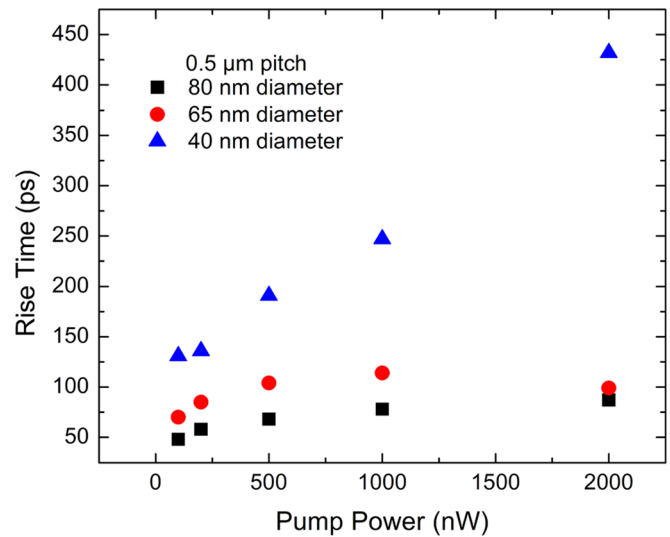


FIG. 10. (Color online) Rise time of QD ensembles with varied QD diameter and fixed pitch of 0.5 μm as a function of pump power.

bottleneck.¹³ However, even in cases where the phonon bottleneck has been experimentally observed, the intra-band relaxation rate is still on the order of tens to hundreds of picoseconds,^{14,15} which is much shorter than the time constant for the carrier transfer from the barrier into the QDs, as indicated by the comparison of GaAs decay times in Fig. 5. Thus, the capture time from the barrier into the QD should dominate the measured rise time of the PL, which supports the hypothesis that the longer rise times observed for smaller QDs results simply from a reduced capture cross-section and not the phonon bottleneck effect. Figure 11 shows a plot of the rise times as a function of the inverse fill factor. The data are strongly nonlinear, indicating that Eq. (3) does not completely describe the physics of the capture process as the diameter of the QD is changed. This is likely due to the fact that once a carrier reaches a QD, the capture process itself is

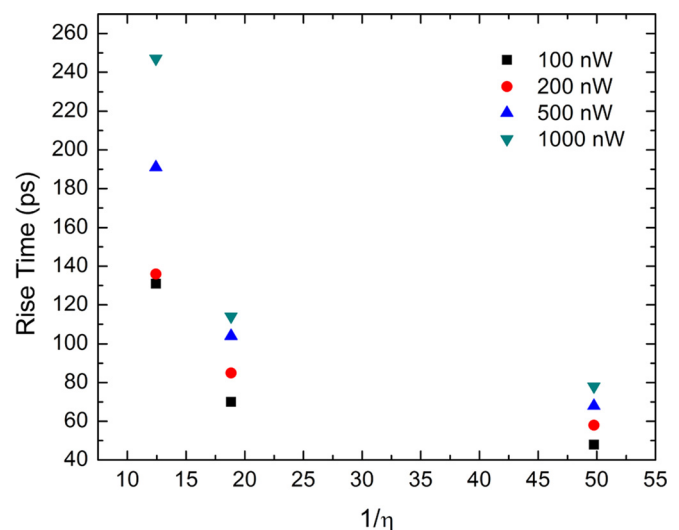


FIG. 11. (Color online) Rise time of QD ensembles with varied QD diameter and fixed pitch of 0.5 μm as a function of inverse fill factor for each of the three arrays with QD diameters of 80, 65, and 40 nm.

fundamentally quantum-mechanical in nature.^{16–18} The development of a model to accurately describe this process is beyond the scope of this work.

In addition, we note the presence of a saturation behavior similar to that observed in Fig. 7 for the two largest QD sizes of 80 and 65 nm. Again, this behavior can be attributed to the more efficient capture rate of these arrays due to their large fill factors that results in the filling of the excited states of the QDs at lower pump powers compared to the array with a 40 nm diameter.

Finally, it is instructive to compare the rise times of lithographically defined quantum dots with the SAQDs. Note that the rise time of approximately 50 ps for the 0.5 μm pitch array in Fig. 7 is comparable to the typical rise time of the SAQD ensembles, despite the significantly lower density of

the lithographically defined QDs. This is likely the result of the fact that the lithographically defined QDs have significantly larger diameters than the SAQDs, and thus the fill factor, η , is comparable to the fill factor of SAQD arrays. The fill factor for the 80 nm diameter QDs on a pitch of 0.5 μm is 0.02. Assuming a SAQD density of 1×10^{10} , we obtain an identical fill factor of 0.02 assuming a diameter of 16 nm, which is a reasonable estimate for typical SAQDs. Thus, the data suggests that the lack of a wetting layer does not play a significant role in the carrier capture rate, but is limited instead by the fill factor of the QD array. Although the lack of a wetting layer does not appear to affect the rise time, it may, however, affect the total number of carriers which are captured by the QDs within the rise time period, or equivalently, the intensity of the QD PL. This supposition is

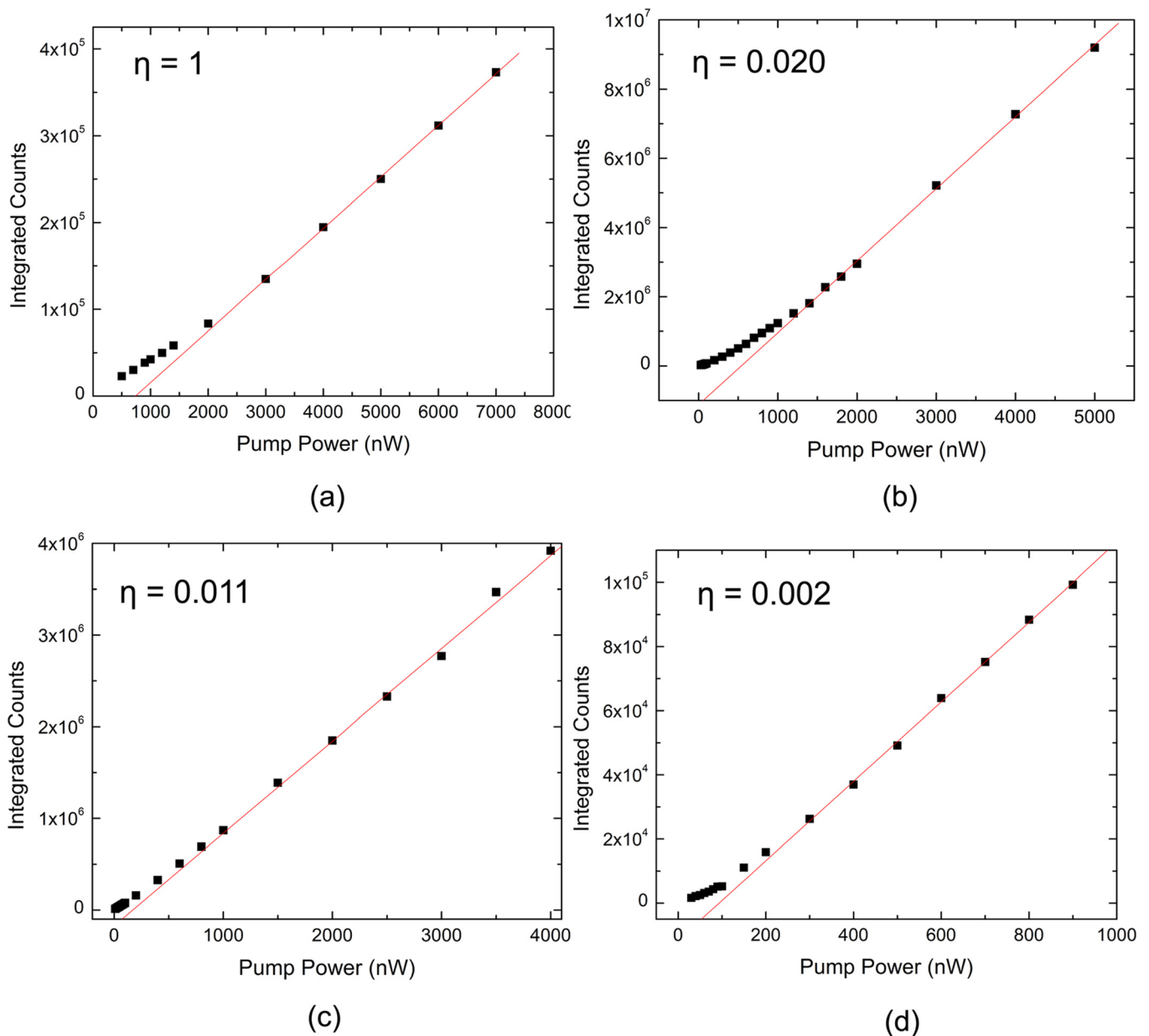


FIG. 12. (Color online) L-L curves obtained from four patterned areas in order of decreasing fill factor η : (a) $2 \times 2 \mu\text{m}^2$ quantum well area, (b) 0.5 μm pitch, 80 nm diameter QD array, (c) 0.5 μm pitch, 60 nm diameter QD array, and (d) 1.6 μm pitch, 80 nm diameter QD array. Solid lines are best fits to the data at pump powers above the critical pump power.

supported by the data comparing the GaAs decay times in Fig. 5, which suggests that the majority of the photogenerated carriers recombine in the GaAs instead of inside the QDs. In the SAQD arrays, the wetting layer efficiently collects carriers from the GaAs due to its large capture cross-section, resulting in a drastic decrease in the GaAs decay time. However, the sum of the transfer time from the GaAs into the wetting layer and the transfer time from the wetting layer into the QDs appears to be comparable to the capture time of a lithographically defined QD array without a wetting layer having a similar fill factor.

C. Decay time of PQD ensembles

As noted in Fig. 3, the PQD luminescence exhibits a bi-exponential decay with a fast component of 300–500 ps and a slow component of 2–2.5 ns. In this section, we present evidence suggesting that the short decay can be attributed to the fast capture of carriers by defect states related to the processing steps, while the slower component can be attributed to the radiative decay of the remaining carriers after saturation of the defect states and continued capture from the GaAs barrier into the QDs at high excitation densities.

Figure 12 shows the total integrated intensity as a function of pump power (L-L curve) for four patterned areas on the same sample. All areas were exposed to identical processing and regrowth conditions. Figure 12(a) shows the L-L curve for a $2 \times 2 \mu\text{m}^2$ quantum well area. For comparison, Figs. 12(b)–12(d) show the L-L curves for three PQD ensembles with different densities and QD diameters. It is clear from Fig. 12 that the L-L curves are nonlinear at low pump powers but become linear at high pump powers. The sublinear increase in intensity in the regime of low pump powers is likely due to the population of defect states related to the processing and regrowth steps. The curves change from sublinear to linear at some critical pump power, at which the defects have been saturated and the additional photogenerated carriers recombine in a predominantly radiative manner.

As shown in Fig. 12, the critical pump power depends on the density of the QD ensemble and the QD diameter. The quantum well area has the largest critical pump power of approximately 3000 nW, followed by the QD array with $0.5 \mu\text{m}$ pitch and 80 nm QD diameter in Fig. 12(b) (~ 1500 nW), the $0.5 \mu\text{m}$ pitch array with 60 nm QD diameter in Fig. 12(c) (~ 1000 nW), and finally the $1.6 \mu\text{m}$ pitch array with 80 nm QD diameter in Fig. 12(d) (~ 300 nW). The larger critical pump power for the quantum well area compared with the QD arrays suggests that the total number of defects is dependent upon the total area of unetched InGaAs material. This might be expected if the defects lie primarily at the top surface of the GaAs cap layer, which is exposed to the PMMA resist and titanium during the processing steps. In the QD-patterned regions, most of this area has been etched away except for the area directly above the QDs themselves, which may lead to a lower total defect density. Figure 13 shows the critical pump power as a function of the fill factor for the three QD arrays in Fig. 12. The linear dependence of the critical pump power on the fill

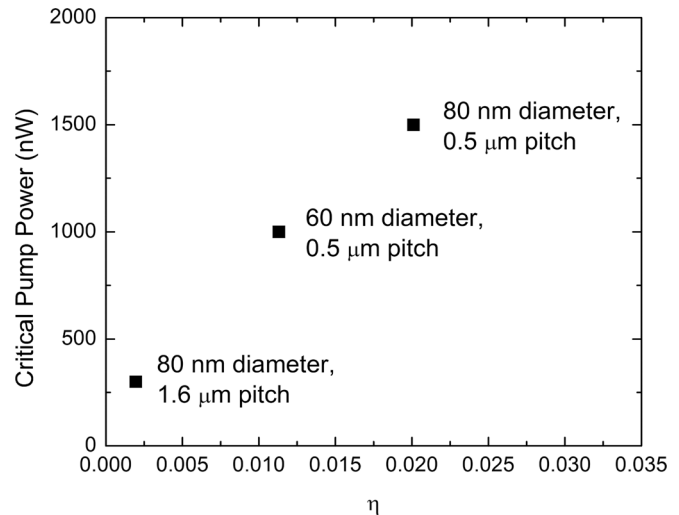


FIG. 13. Critical pump power for the three QD arrays in Fig. 12 as a function of the fill factor for each array.

factor supports the area dependence of the number of processing-induced defects.

Figure 14 shows the TRPL traces at various pump powers obtained from the four patterned areas in Fig. 12. Comparing Fig. 14(a) with Figs. 14(b)–14(d), we note that the initial fast decay time of the quantum well area (~ 100 ps) is much shorter than any of the QD-patterned areas (400–500 ps), and is also shorter than the exciton lifetimes typically observed in InGaAs quantum wells grown by MBE (~ 400 ps).¹⁹ This observation is consistent with the strong nonlinearity observed in the L-L curve for the quantum well area in Fig. 12(a), which suggests a larger number of total defects for the quantum well area compared to the QD-patterned areas. In addition, at comparable pump powers the tail of the quantum well luminescence is much less prominent than the tail of the QD luminescence, suggesting that even at the highest pump powers investigated, the defects in the quantum well area are not completely saturated. In the QD-patterned areas the smaller total number of defects results in a saturation of the defects at moderate pump powers, making the long-lived tail more prominent in comparison to the quantum well.

D. Temperature dependence

Analysis of the QD TRPL at temperatures above 4 K can reveal additional information about the presence of defect states and the threshold for thermionic emission from the QDs into the barrier. The TRPL from an array of 50 nm diameter QDs on a pitch of $0.5 \mu\text{m}$ was investigated at temperatures ranging between 4 and 100 K. The pump power was held fixed at $1 \mu\text{W}$ for all measurements. Figures 15 and 16 show the spectra and TRPL from this array at temperatures between 10 and 80 K. The spectra exhibit the expected broadening and redshift typical of high temperatures.

Qualitatively, we note that the long tail of the PL becomes less prominent as the temperature is increased. At 10 K, the fast and slow components of the decay are clearly distinct, while at 80 K the TRPL is completely dominated by

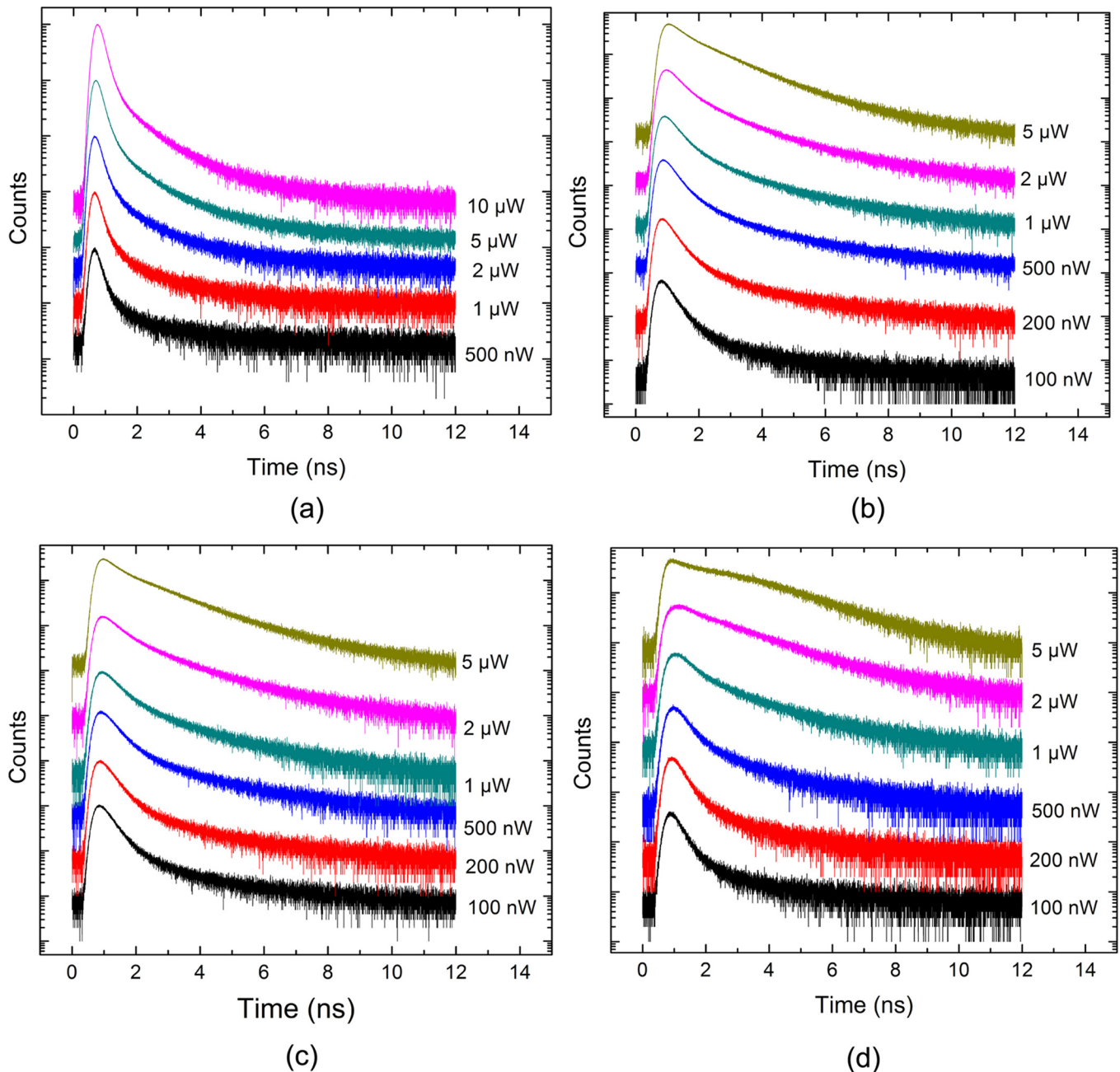


FIG. 14. (Color online) Time-resolved photoluminescence traces from the four patterned areas in Fig. 10: (a) $2 \times 2 \mu\text{m}^2$ quantum well area, (b) $0.5 \mu\text{m}$ pitch, 80 nm diameter QD array, (c) $0.5 \mu\text{m}$ pitch, 60 nm diameter QD array, and (d) $1.6 \mu\text{m}$ pitch, 80 nm diameter QD array.

the fast decay. These results are in agreement with the interpretation of the fast decay resulting from defect states, while the slow decay results from the radiative recombination inside the QD and refilling of the QD from the barrier. A detailed theoretical analysis of the tunneling rates from a QD into the surrounding defects predicts an increase in the tunneling rate of 2 orders of magnitude as the temperature is increased from 4 to 300 K,²⁰ which is consistent with the observation that the fast decay dominates over the long tail at higher temperatures.

Figure 17 shows the rise times and fast decay times of the TRPL curves in Fig. 16. Both rise and decay times exhibit an increase up to 60 K followed by a drop at higher

temperatures. As was previously discussed, the carrier capture process and hence, the rise time is determined by carrier drift within the GaAs barrier. The increase in rise time as the temperature is increased is consistent with a higher thermal velocity of carriers in the barrier, resulting in a higher capture rate by the QDs according to Eq. (2). Based on Eq. (2), one might expect a square-root dependence of the rise time on the temperature, which does not appear to apply to the data in Fig. 17. However, as we have shown in Fig. 7, high-density arrays exhibit a saturation of the rise time even at relatively low pump powers on the order of hundreds of nanowatts. At a pump power of $1 \mu\text{W}$, we are clearly generating enough carriers to occupy the excited states of the QDs in

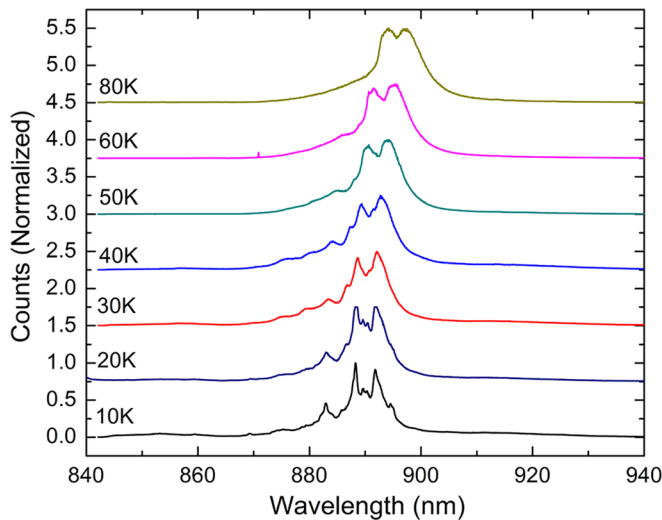


FIG. 15. (Color online) Temperature dependent PL spectra from a QD array with a pitch of $0.5 \mu\text{m}$ and 50 nm diameter.

the array, as shown by the spectra in Fig. 15. The saturation of the rise time is likely obscuring the simple square-root dependence of the rise time one would expect from Eq. (2), which may more accurately represent the data at significantly lower pump powers before the onset of saturation. However, the fast decay time constant does, in fact, increase in direct proportion to the square root of the temperature. The carrier capture rate by defects directly from the GaAs barrier can be represented by an equation identical to Eq. (2).²⁰ Thus, we should expect the rate at which carriers occupy the defect states to follow a similar square-root dependence of the temperature. The faster saturation of these defects as the temperature is increased leads to a longer decay time constant of the radiative emission from the QDs.

At 60 K, the thermal energy kT is $\sim 5 \text{ meV}$, on the order of the separation between confined conduction band states in a QD with a diameter of 50 nm . Thus, the decrease in rise and decay times at temperatures above 60 K is likely due to

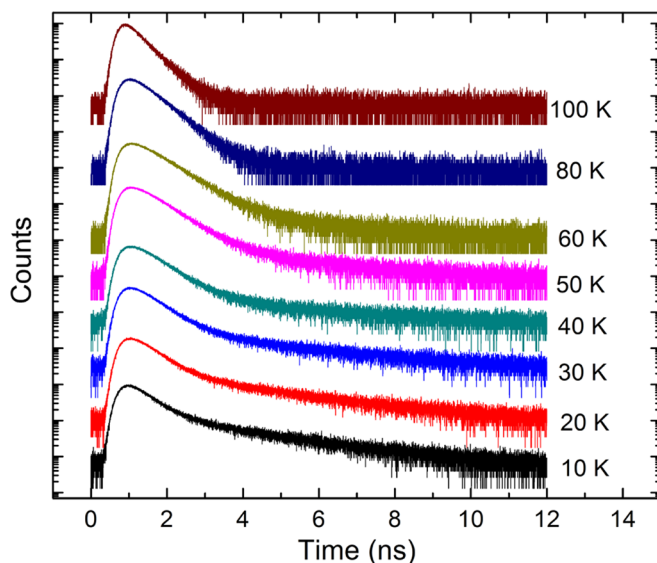


FIG. 16. (Color online) TRPL traces from the QD array in Fig. 15 at various temperatures ranging between 10 and 100 K.

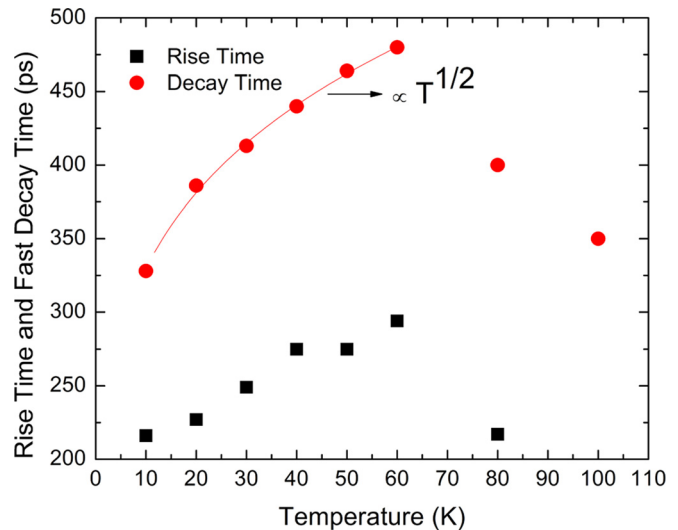


FIG. 17. (Color online) Rise time and fast decay time of the TRPL traces in Fig. 16. The solid line is a fit to a function of the form $a + bT^{1/2}$.

thermionic emission into excited states of the QD and the barrier.

IV. CONCLUSION

We have performed a systematic investigation of the time-resolved photoluminescence from patterned quantum dot arrays. Measurements of the rise time as a function of the QD density and diameter indicate that the carrier capture process is relatively slow in comparison to SAQDs, and is limited by the carrier drift velocity in the bulk GaAs barrier. Similar measurements of the decay time as a function of the QD density and diameter, along with L-L curves for different QD arrays, suggest that the fast component of the decay is the result of capture by nearby defect states, while the longer tail is the result of the radiative decay of the remaining carriers and repopulation from the GaAs barrier.

These results will be important for improving the quality of single-photon sources based on patterned QDs. The area dependence of the defect density suggests that these defects may potentially be eliminated by performing a short etch-back of the GaAs cap layer to remove processing-induced defects before the regrowth of the GaAs barrier material. Alternatively, the thickness of the GaAs cap could be increased to reduce the interaction of the QD wavefunction with the defects. Doubling the thickness of the GaAs cap layer from 10 to 20 nm should result in a reduction of more than 4 orders of magnitude in the tunneling rates, as predicted by Sercel.²⁰

Finally, our investigation of the temperature at which thermionic emission becomes important suggests that the efficiency of a single-photon emitting device utilizing a single patterned quantum dot will begin to degrade above a temperature of approximately 60 K for the particular fabrication process and epitaxial structure used for this work.

ACKNOWLEDGMENTS

The authors thank Todd Harvey for assistance with the MBE growth. The work at Illinois was supported by the U.S.

Department of Energy, Office of Basic Energy Sciences as part of an Energy Frontier Research Center and the National Science Foundation (Grant No. ECCS 08-21979).

- ¹M. Henini and M. Bugajski, *Microelectron. J.* **36**, 950 (2005).
²R. P. Mirin, *Appl. Phys. Lett.* **84**, 1260 (2003).
³C. Santori, D. Fattal, J. Vuckovic, G. S. Solomon, and Y. Yamamoto, *New J. Phys.* **6**, 89 (2004).
⁴P. Michler, A. Kiraz, C. Becher, W. V. Schoenfeld, P. M. Petroff, L. Zhang, E. Hu, and A. Imamoglu, *Science* **22**, 2282 (2000).
⁵V. B. Verma and J. J. Coleman, *Appl. Phys. Lett.* **93**, 111117 (2008).
⁶V. B. Verma, U. Reddy, N. L. Dias, K. P. Bassett, X. Li, and J. J. Coleman, *J. Quantum Electron.* **46**, 1827 (2010).
⁷V. B. Verma, M. J. Stevens, K. L. Silverman, N. L. Dias, A. Garg, J. J. Coleman, and R. P. Mirin, *Opt. Express* **19**, 4182 (2011).
⁸B. Ohnesorge, M. Albrecht, J. Oshinowo, A. Forchel, and Y. Arakawa, *Phys. Rev. B* **54**, 11532 (1996).
⁹D. Morris, N. Perret, and S. Fafard, *Appl. Phys. Lett.* **75**, 3593 (1999).
¹⁰Y. Toda, O. Moriwaki, M. Nishioka, and Y. Arakawa, *Phys. Rev. Lett.* **82**, 4114 (1999).
¹¹T. Nielsen, P. Gartner, and F. Jahnke, *Phys. Status Solidi C* **0**, 1532 (2003).
¹²S. Marcinkevičius and R. Leon, *Physica B* **272**, 36 (1999).
¹³H. Benisty, C. M. Sotomayor-Torrès, and C. Weisbuch, *Phys. Rev. B* **44**, 10945 (1991).
¹⁴T. Kitamura, R. Ohtsubo, M. Murayama, T. Kuroda, K. Yamaguchi, and A. Tackeuchi, *Phys. Status Solidi C* **0**, 1165 (2003).
¹⁵J. Urayama, T. B. Norris, J. Singh, and P. Bhattacharya, *Phys. Rev. Lett.* **86**, 4930 (2001).
¹⁶T. R. Nielsen, P. Gartner, and F. Jahnke, *Phys. Rev. B* **69**, 235214 (2004).
¹⁷U. Bockelmann and T. Egeler, *Phys. Rev. B* **46**, 15574 (1992).
¹⁸A. V. Uskov, F. Adler, H. Schweizer, and M. H. Pilkuhn, *J. Appl. Phys.* **81**, 7895 (1997).
¹⁹Th. Amand, X. Marie, B. Dareys, J. Barrau, M. Brousseau, D. J. Dunstan, J. Y. Emery, and L. Goldstein, *J. Appl. Phys.* **72**, 2077 (1992).
²⁰P. C. Sercel, *Phys. Rev. B* **51**, 14532 (1995).